Theoretical Raman Optical Activity Study of the β Domain of Rat Metallothionein

Sandra Luber and Markus Reiher*

Laboratorium für Physikalische Chemie, ETH Zürich, Wolfgang-Pauli-Str. 10, CH-8093 Zürich, Switzerland

Received: October 2, 2009; Revised Manuscript Received: November 3, 2009

We present the calculated vibrational Raman optical activity (ROA) spectrum of the β domain of rat metallothionein, which is the by far largest molecule for which full ab initio ROA calculations have been performed up to date with more than 400 atoms. While ROA signatures of regular secondary structure elements like β-sheets and α-helices can be conveniently studied in terms of small model structures, this is no longer possible for more irregular proteins like metallothionein. The only secondary structure elements occurring in the molecule are turns, in particular β turns. Our calculations reveal that especially bands in the wavenumber range from about 1100 to 1400 cm^{-1} may be employed as signatures of such β turns. This is also found in comparison to experimental data. In addition, good agreement between calculated and experimental spectra is found.

1. Introduction

Metallothioneins are cysteine-rich proteins, which have been known since 1957.[1] They have the ability to bind heavy metals, mainly zinc, but also others like cadmium, copper, mercury, silver, and arsenic.[2] Their metabolic role is still not totally clear,[1] and their functions in organisms have been discussed extensively in the literature (for an overview, see, e.g., refs 1, 3, 4). For instance, metallothioneins play an important role in zinc-transfer processes and corresponding redox reactions.[5−7] Moreover, they quench reactive oxygen and nitrogen molecules, causing oxidative stress, and they have been investigated in the context of diseases like diabetes, rheumatoid arthritis, and atherosclerosis as well as Parkinson, Creutzfeldt−Jacob, and Alzheimer.[1,8−10]

Four different forms have been identified in mammals, which all contain 20 cysteine and at least five lysine residues. The amino acids histidine, phenylalanine, tyrosine, and tryptophan have not been found. As a consequence, metallothioneins do not adsorb radiation around 280 nm, which is usually applied in routine methods of protein detection.[1] X-ray and nuclear magnetic resonance (NMR) studies have revealed that metallothioneins consist of an α and a β domain, the first containing 11 cysteine residues with four metal atoms and the other binding three metal ions with the help of nine cysteine residues.[11−16] The dominating secondary structure elements are β turns, which consist of four amino acid segments. Vibrational spectroscopy like infrared (IR) and Raman spectroscopy and their chiral variants vibrational circular dichroism (VCD)[17] and vibrational Raman optical activity (ROA)[18−20] also provide information about the structure of metallothioneins in their natural environment. The spectra, however, are often difficult to understand so that, in addition, theoretical investigations are required. This combined approach has already facilitated the interpretation of experimental IR, Raman, and VCD spectra of metallothioneins (see, e.g., ref 21). There is one ROA spectrum available, measured by Smyth et al. from rabbit metallothionein.[22] This spectrum contains some interesting bands, which could not be assigned with certainty to the structural features and the corresponding normal modes. Here, a calculation can yield deeper insights, clarifying the origin of these bands. Until recently, full ab initio ROA calculations could, however, only deal with quite small molecules due to the high computational effort (for example, see refs 23−37). The employment of density-fitting techniques[38−40] for ROA property calculations[41] has now made the calculation of larger molecules feasible.[42−47] Employing this approach, we present ROA calculations for the β domain of rat metallothionein, for which already a molecular dynamics study has been presented.[48] This metallothionein has been chosen since a refined X-ray structure of rat metallothionein is available.[14] A graphical representation of the optimized structure is shown in Figure 1. The overall structure contains in total more than 400 atoms with 31 amino acid residues. This

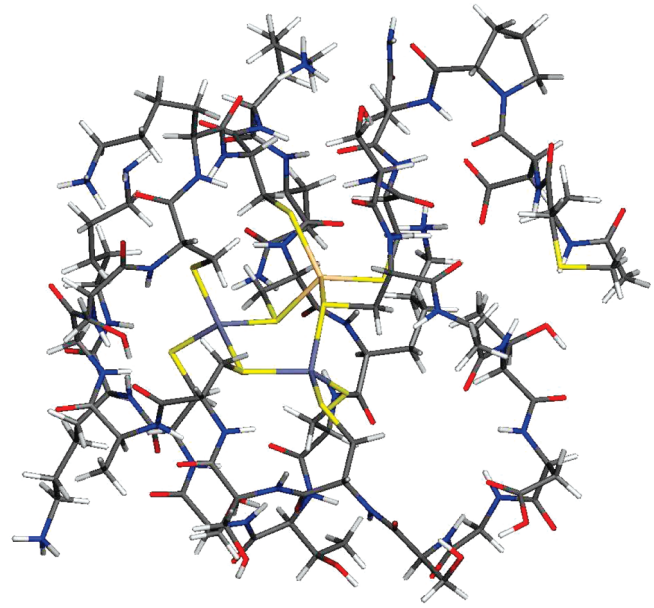

Figure 1. Graphical representation of the optimized structure (BP86/RI/TZVP) of the β domain of rat metallothionein employed in the calculations; hydrogen atoms are indicated by white, nitrogen atoms by blue, carbon atoms by gray, oxygen atoms by red, and sulfur atoms by yellow. The metal ions clustered by the cysteine residues are two zinc and one cadmium ion, which are given in gray and yellow, respectively.

* To whom correspondence should be addressed. E-mail: markus.reiher@phys.chem.ethz.ch. Fax: +41-44-63-31594.

10.1021/jp909483q
Published on Web 12/16/2009

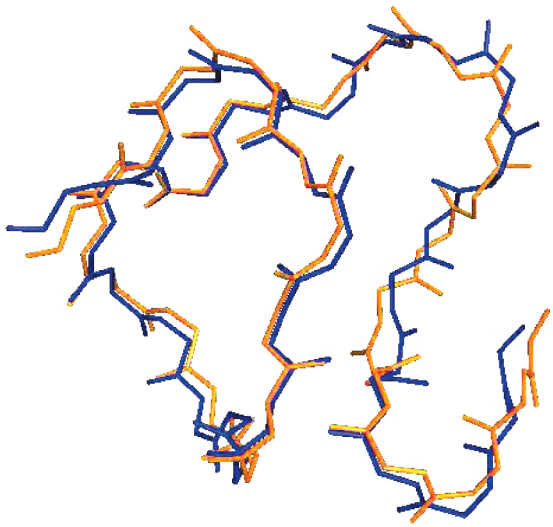

Figure 2. Graphical representation of the backbone trace of the β domain crystal structure (PDB code 4mt2) in blue and of the optimized structure (BP86/RI/TZVP) in orange.

molecule has an irregular structure and is therefore an example of a system to which computationally cheaper, approximate theoretical approaches for ROA spectra calculations employing results of smaller fragments for the extrapolation to larger molecular systems[49] cannot be applied.

The paper is organized as follows: after the computational methodology in section 2, the model structure employed for the calculations is discussed in section 3. The calculated ROA spectrum is presented in section 4, followed by a comparison of experimental and calculated Raman and ROA spectra in section 5. A summary can be found in section 6.

2. Computational Methodology

The structure optimization was carried out by the program package Turbomole[50] employing density functional theory with the density functional BP86[51,52] and Ahlrichs' TZVP basis set.[53] The same density functional and basis set were used for the vibrational spectra calculations, which were performed as described in ref 41 with Snf[54] in combination with Turbomole for the electronic energy gradient calculation and our local version of Turbomole's escf module for the ROA property tensor evaluation.[41] The resolution-of-the-identity density-fitting technique was employed in all calculations. Since the theoretical foundation for the intensity calculations performed in this work is the far-from-resonance approximation, any resonance with electronic states has to be avoided. That is why a laser wavelength of 1800 nm was chosen. Solvent effects were not taken into account. The structural pictures were produced with PyMOL[55] and Ramachandran plots with the Protein Structure Validation Suite[56] employing MolProbity.[57]

3. Comparison of the Crystal and the Model Structure

The starting coordinates for the structure optimization were taken from the X-ray structure of rat metallothionein (PDB code 4mt2)[11,12,14,15] by omitting the α domain part. In order to assess how much the structure employed in the spectra calculation deviates from the β domain of the rat metallothionein crystal structure, a superposition of the backbone trace of the optimized and the crystal structure is shown in Figure 2.

The backbone of the optimized structure is quite similar to that of the crystal structure. Some larger deviations are obvious, especially at the ends of the backbone. The only secondary structure elements found in the β domain of the crystal structure are β turns, which are defined by four sequential amino acid residues. Employing the backbone torsional angles ϕ and ψ, which correspond to the C−N−C$^{\alpha}$−C and N−C$^{\alpha}$−C−N dihedral angles, several types of turns have been defined: type I is classified by ideal angles of $\phi_{i+1} = -60°$ and $\psi_{i+1} = -30°$ on residue $i + 1$ and $\phi_{i+2} = -90°$ and $\psi_{i+2} = 0°$ angles on residue $i + 2$, where i denotes the first atom constituting the turn. Type II is defined by $\phi_{i+1} = -60°$, $\psi_{i+1} = 120°$, $\phi_{i+2} = 80°$, and $\psi_{i+2} = 0°$, type VIII by $\phi_{i+1} = -60°$, $\psi_{i+1} = -30°$, $\phi_{i+2} = -120°$, and $\psi_{i+2} = 120°$, type I′ by $\phi_{i+1} = 60°$, $\psi_{i+1} = 30°$, $\phi_{i+2} = 90°$, and $\psi_{i+2} = 0°$, and type II′ by $\phi_{i+1} = 60°$, $\psi_{i+1} = -120°$, $\phi_{i+2} = -80°$, and $\psi_{i+2} = 0°$. Type IV contains in our case all turns which are excluded from these categories (for further details, we refer to refs 58−61). A β turn of type I is found for residues Asp2−Pro3($\phi = -58°$; $\psi = -36°$)−Asn4 ($\phi = -86°$; $\psi = -14°$)−Cys5 and the sequence Cys26 −Thr27($\phi = -71°$; $\psi = -12°$)−Ser28($\phi = -79°$; $\psi = -10°$)−Cys29. The residues Cys15−Ala16($\phi = 33°$; $\psi = 63°$)−Gly17($\phi = 77°$; $\psi = 6°$)−Ser18 and Cys21−Lys22($\phi = -76°$; $\psi = -45°$)−Gln23($\phi = -146°$; $\psi = 75°$)−Cys24 form a β turn of type I′ and IV, respectively. The dominating secondary structure elements in the α domain of the rat metallothionein (not shown) are also β turns, where several turns of type I and one of type IV are detected in addition to one inverse γ turn.

Similar results are obtained for the optimized structure. The turns of type I are found with angles of $\phi = -85°$ and $\psi = 10°$ for Pro3, respectively, $\phi = -106°$ and $\psi = -7°$ for Asn4, as well as $\phi = -81°$ and $\psi = 2°$ for Thr27 and $\phi = -100°$ and $\psi = 1°$ for Ser28. The I′ β turn shows now angles of $\phi = 52°$ and $\psi = 44°$ for Ala16 and $\phi = 88°$ and $\psi = 2°$ for Gly17. The sequence giving rise to a IV β turn in the crystal structure forms a β turn of type IV in our optimized structure with $\phi = -109°$ and $\psi = -57°$ for Lys22 and $\phi = -132°$ and $\psi = 97°$ for Gln23. In addition, a type IV β turn is determined for the residues Pro3−Asn4($\phi = -106°$; $\psi = -7°$) −Cys5($\phi = -133°$; $\psi = 92°$)−Ser6. As in the α domain of the crystal structure, an inverse γ turn is ascertained constituted by Ala8−Thr9($\phi = -87°$; $\psi = 78°$)−Asp10.

Ramachandran plots[62] of the β domain of both the crystal structure and the optimized structure are presented in Figure 3.

In both structures, almost all amino acid residues show ϕ and ψ angles in the favored regions. The number of residues in the α region, which contains values of about $\psi = 40°$ to $-60°$ and in which the α and 3_{10} helices are found, is more or less as high as the quantity of amino acids in the β regions belonging to higher ψ values. One residue (except for the glycine residues) carries a positive ϕ value in the left-handed helix region. These results demonstrate that the optimized structure shows all important secondary structure elements as the corresponding crystal structure, although the latter may, of course, deviate from the structure occurring in solution. A similar disordered structure and ψ/ϕ angle distribution is found for the α domain of the crystal structure. Therefore, we only take the β domain into account for our calculations, which results also in a lower computational effort.

4. Analysis of the Calculated ROA Spectrum

The calculated ROA spectrum of the β domain of rat metallothionein is presented in Figure 4. The most intense bands occur in the region from about 1180 to 1420 cm^{-1}. A number of mostly positive bands is obvious at low wavenumbers, where skeletal vibrations occur. The one at around 750 cm^{-1} arises

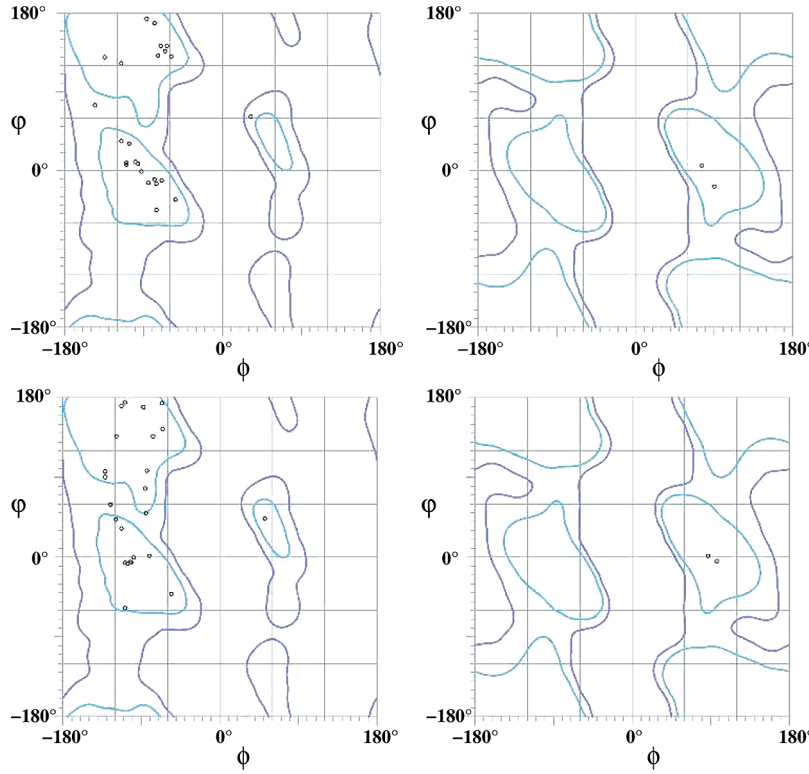

Figure 3. Ramachandran plots of the glycine residues (right-hand side) and the remaining amino acids (left-hand side); ϕ is the C−N−C$^{\alpha}$−C and ψ the N−C$^{\alpha}$−C−N dihedral angle; the upper part belongs to the β domain of the crystal structure (PDB code 4mt2) and the lower one to the corresponding optimized structure (BP86/RI/TZVP); the light blue lines indicate favored and the dark blue lines allowed regions of the ϕ/ψ dihedral angle combinations (for details, see ref 68).

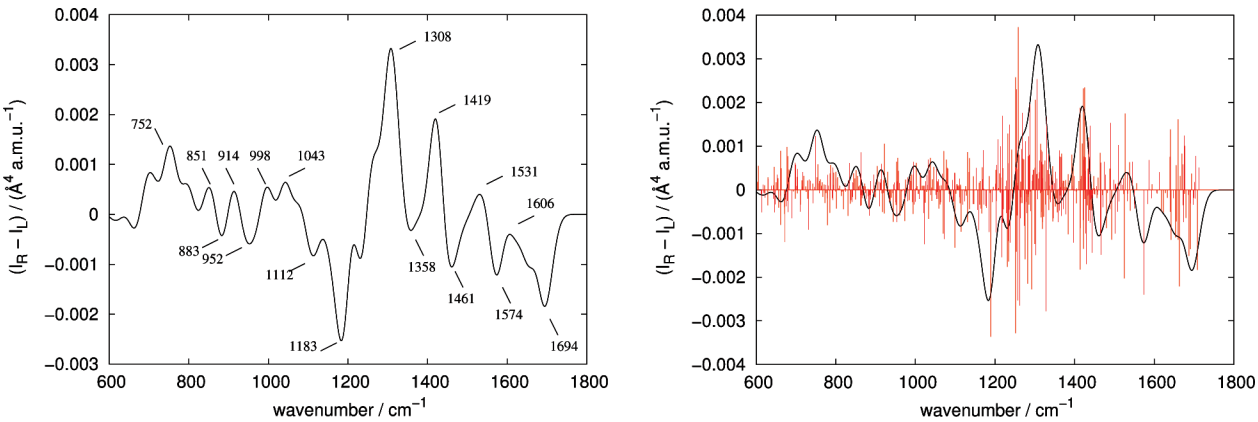

Figure 4. Calculated backscattering ROA spectra (BP86/RI/TZVP) of the β domain of rat metallothionein [broadened with a Gaussian band shape (full width at half height: 40 cm^{-1})] on the left-hand side and with the line spectrum (scaled by 0.04) on the right-hand side.

due to deformational vibrations of the carbon atoms with a large contribution of an out-of-plane motion of the hydrogen atoms bound to the nitrogen atoms, especially of the cysteine residues. These out-of-plane modes together with the backbone vibrations also give rise to positive ROA intensities around 800 cm^{-1}, including the hydrogen atoms from other amino acids like the hydroxyl hydrogen atoms of threonin and serine residues. Deformational hydrogen vibrations, in particular of the methyl and methylene groups, distributed over the whole molecule and coupled with stretching vibrations of the backbone result in the positive band at 851 cm^{-1}.

The small negative band at 883 cm^{-1} is mainly due to the normal mode at 884 cm^{-1}, which features an in-plane deformational vibration of two cysteine residues bound to a zinc atom (see Figure 5), whereas the positive band around 910 cm^{-1} contains an important contribution of, e.g., lysine C−N stretching vibrations.

The negative contributions around 950 cm^{-1} arise from delocalized C−C stretching vibrations, e.g. at 953 cm^{-1} from the Gly11 residue. A significant negative ROA intensity shows the normal mode at 1022 cm^{-1}, which is more or less located on Cys13 with a strong C−C stretching vibration between the carbon atom of the methylene group and C$^{\alpha}$. Contrary to that, the stretching between C−O of Ser14 at 1032 cm^{-1} as well as the serine vibration at 1046 cm^{-1} (see Figure 5) and the C−C stretching modes of Cys21 at 1037 cm^{-1} and Lys20 at 1059 cm^{-1} contribute remarkable positive ROA intensities. The C−C and C−O stretching vibrations of the serine residues give rise to positive and negative contributions at 1070 and 1071 cm^{-1}, respectively. A large part to the negative band observed around 1110 cm^{-1} is provided by the backbone stretching and hydrogen wagging and twisting vibrations of Lys30 and Lys31 at 1072 cm^{-1} and of Lys20 at 1115 cm^{-1} (compare Figure 5). The most negative ROA intensity, which also brings about the most

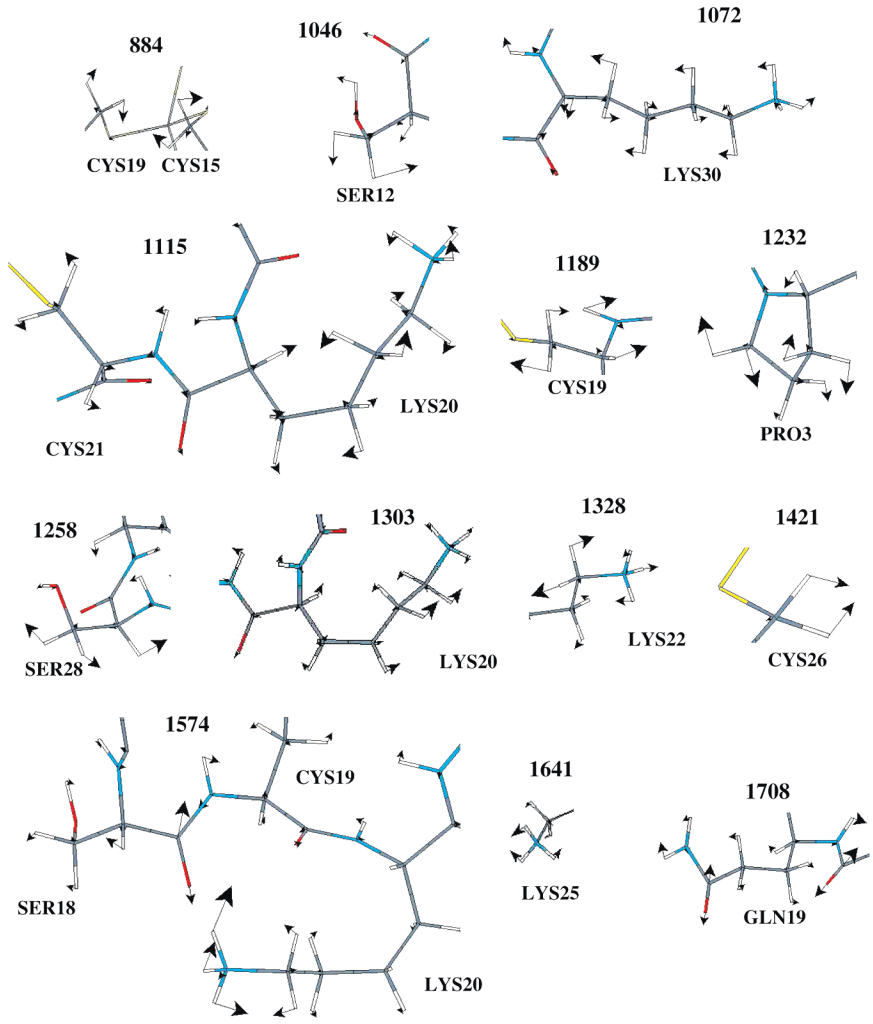

Figure 5. Characteristic normal modes of structural fragments; the numbers indicate the corresponding wavenumbers in cm^{-1}.

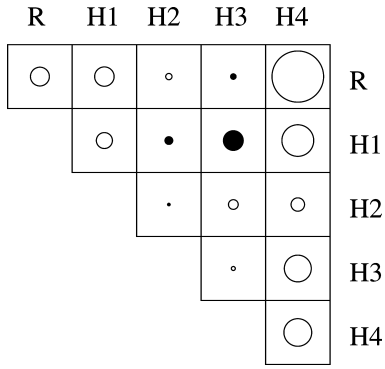

Figure 6. Group coupling matrix for the $\beta(G')^2$ invariant of the normal mode at 1189 cm^{-1} for the β domain of rat metallothionein; "H1" and "H2" denote the hydrogen atoms of the methylene group, and "H3" and "H4" the hydrogen atoms bound to C^{α} and the nitrogen atom of Cys19, respectively. The contributions of the remaining atoms of the molecule are summarized in "R".

negative band in the broadened spectrum in Figure 4, is found for the normal mode of Cys19 at 1189 cm^{-1} shown in Figure 5. It is dominated by the amide III vibration, i.e., by the bending vibration of the hydrogen atom on the nitrogen and C^{α} atom, together with methylene twist motions. A local decomposition of this normal mode depicted by a group coupling matrix as proposed by Hug[63] is shown in Figure 6 for the $\beta(G')^2$ invariant, for which a large negative value has been calculated. For the electric-quadrupole-containing invariant, solely a negligibly small negative intensity value has been evaluated so that its contribution to the backscattering ROA intensity can safely be neglected. The rows and columns of the matrix in Figure 6 correspond to atoms or groups of atoms. The magnitude of their contribution is represented by the area of circles, which are filled if the sign of the contribution is positive and empty if negative. As can be seen in Figure 6, the large negative intensity found for this normal mode is basically due to the contributions from the hydrogen atom bound to the nitrogen atom. Not only does the hydrogen atom itself provide a remarkable negative value, but also its coupling to the neighboring hydrogen atoms and the remaining molecule. Smaller negative contributions are evaluated especially for one hydrogen atom of the methylene group, whereas the hydrogen atom of C^{α} gives rise to predominantly, yet comparatively small, positive contributions.

Significant positive ROA intensities are found for the amide III modes of, for example, Ser6 at 1207 cm^{-1}, Lys30 and Tyr27 at 1214 cm^{-1}, Asp2 at 1219 cm^{-1}, and Lys30 and Lys31 at 1236 cm^{-1}. In contrast to that, negative intensity values are calculated, for instance, for Thr27 and Cys26 at 1185 cm^{-1}, Cys7 at 1202 cm^{-1}, Lys20 and Cys21 at 1231 cm^{-1}, and Asp10, Gly11, and Ser12 at 1234 cm^{-1}. Twist motions of Pro3 at 1232 cm^{-1} (see Figure 5) and 1252 cm^{-1} also show nonnegligible positive and negative ROA intensities, respectively. The broad band with maximum at 1308 cm^{-1} and the small minimum at 1358 cm^{-1} in Figure 4 encompass more or less C^{α}−H bending vibrations. Two different types can be distinguished: one with

a motion of the hydrogen atom perpendicular to the direction of the $C^{\alpha}-N$ bond, designated as $C^{\alpha}-H(II)$, occurring from about 1250 to 1300 cm^{-1} and one with the hydrogen atom moving along this bond, indicated by $C^{\alpha}-H(I)$, observed in the region from about 1300 to 1330 cm^{-1}.[43,64,47] Negative contributions from such modes originate, for example, from Gly11 at 1257 cm^{-1}, Gly17 and Ser18 at 1262 cm^{-1}, Cys29 at 1292 cm^{-1}, and lysine residues at 1303 and 1328 cm^{-1} (see Figure 5). Positive contributions worth mentioning are from Cys13 and Ser14 at 1254 cm^{-1}, Cys19 at 1288 cm^{-1}, Ser12 at 1301 cm^{-1}, and Lys20 and Lys22 at 1305 and 1330 cm^{-1}, respectively. The highest ROA intensity calculated in the plotted wavenumber range in Figure 4 shows the normal mode at 1258 cm^{-1}, which is dominated by the $C^{\alpha}-H(II)$ normal mode of Ser28 and contributions from methylene wagging vibrations mainly of the cysteine residues (see Figure 5). It does, nevertheless, not lead to the most intense band due to overlap with bands of other (negative) ROA intensities. Thus, the maximum is observed at 1308 cm^{-1} in the calculated spectrum, mainly due to the $C^{\alpha}-H(II)$ modes of the lysine residues.

Bending vibrations, especially from the methyl group in combination with the hydroxyl hydrogen atom of Lys22, lead to a remarkable negative ROA intensity at 1414 cm^{-1}, whereas the methylene bending modes of, for example, Lys30 at 1414 cm^{-1}, several cysteine residues at 1422 cm^{-1} (see Figure 5), and Asp2 at 1424 cm^{-1} provide positive contributions so that in total a positive band at around 1420 cm^{-1} is observed. The reasons for the negative band around 1460 cm^{-1} are in particular the negative ROA intensities from Lys20 methylene bending and Lys30 amino group wagging modes. The Lys22 methylene bending and Lys20 wagging vibration at 1474 and 1490 cm^{-1}, respectively, comprise, however, a large positive ROA intensity. Typical amide II modes, i.e., a strong bending of the hydrogen atom bound to the nitrogen atom as well as C−N stretching, is observed at 1480 cm^{-1} for Lys30 and Lys31 and at 1502 cm^{-1} for Lys20 with a remarkable negative intensity. Contrary to that, Ser14 together with Cys13 and Cys15 show amide II modes with a nonnegligible positive value at 1510 cm^{-1} and Ala16 in combination with Ser14 and Cys15 an even more intense one at 1527 cm^{-1}. Positive contributions are also found at, for example, 1538 and 1545 cm^{-1} from amide II modes of Ser6 and Cys21, respectively, so that a small positive band at around 1531 cm^{-1} in Figure 4 is obtained despite the large negative ROA intensity provided at 1524 cm^{-1} (compare the line spectrum at the right-hand side of Figure 5) from the Cys29, Ala16, and Gly17 amide II modes.

Quite a few normal modes are obtained in the region from about 1550 to 1620 cm^{-1}. The by far largest (negative) ROA intensity comprises the mode at 1574 cm^{-1}, which is dominated by C−N and carbonyl stretching vibrations of Lys20 and wagging vibrations of Ser18. A graphical representation of this normal mode can be found in Figure 5. The remaining normal modes up to 1800 cm^{-1} are either wagging vibrations of the Lys NH_3 groups or typical amide I vibrations, which are characterized by carbonyl stretching motions with smaller contributions from N−H and $C^{\alpha}-H$ bending modes. Significant positive ROA intensities are, for example, obtained for Lys25 and Lys20 wagging modes at 1641 (see Figure 5) and 1660 cm^{-1} while Lys22 and Lys25 at 1642 cm^{-1} and Lys22 wagging modes at 1660 cm^{-1} lead to remarkable negative intensities. Noteworthy positive contributions from amide I modes are calculated for Lys25 and Cys26 at 1677 cm^{-1}, Cys13 and Ser14 at 1669 cm^{-1}, and Met1 and Asp2 at 1676 cm^{-1}. Nevertheless, the negative contributions prevail and occur for amide I modes for instance at 1654 cm^{-1} for Ala8 and Thr9, at 1662 cm^{-1} for Cys24 and GLN23, at 1687 cm^{-1} for Gly11, at 1691 cm^{-1} for Ala16, and at 1709 cm^{-1} for Cys21 and Lys22 (see Figure 5 for a graphical representation of the vibration).

5. Comparison to Experimental Spectra

As a final step, we compare our calculated spectra to the measured ROA and Raman spectra of rabbit metallothionein presented in ref 22. It is expect that there will be some differences since our calculation considers the β domain of rat metallothionein in the gas phase, whereas the experiment has been performed for rabbit metallothionein, which has the same amino acid sequence as rat metallothionein but contains seven cadmium metal atoms instead of two zinc and five cadmium atoms, in a pH = 8 buffer solution. In addition, the cadmium ions are kinetically labile, which easily leads to dimerization of the metallothionein in the sample. As a consequence, 28% dimer was found after the ROA measurement of the rabbit metallothionein in the solution.[22]

Comparing the lower wavenumber part of the experimental and calculated ROA spectra shown in the upper part of Figure 7, some similarities are visible. A positive band in the experimental spectrum at around 750 cm^{-1} is also found in the calculated spectrum as well as the following minimum. The doublet around 1000 cm^{-1} in our calculated spectrum, originating mainly from backbone stretching modes, agrees with the one in the experimental spectrum with maxima at 974 and 1016 cm^{-1}. The most obvious bands in the experimental spectrum are the negative band at 1201 cm^{-1} and the positive one with maximum at 1313 cm^{-1}. These are astonishingly well reproduced in our calculation. As has been shown in the previous section, the sharp negative band is due to vibrations of cysteine residues, which has not totally been clear from analyzing the experimental spectrum only.[22] The positive band in the experimental spectrum, which has a slightly broader shoulder at the lower wavenumber side, was assumed to exist due to residues with ψ and ϕ angles in the α region of the Ramachandran plot, whereas β structures were supposed to be absent due to missing negative ROA bands in the 1220−1260 cm^{-1} region.[22] The corresponding band in our calculation is broadened to the lower wavenumber region, since it contains two types of vibrations: amide III modes at lower wavenumbers and $C^{\alpha}-H$ bending vibrations at higher ones. Looking at significant contributions to the intensity with respect to the different amino acids (compare the previous section) and the corresponding ϕ and ψ angles, no relation between the sign of the intensity and these angles is obvious. As a consequence, no general statement about the sign of the band and the occurrence of particular amino acids and backbone angles can be made. However, since our model structure contains turns as the only secondary structure elements, these two bands may be considered as signatures for turns, especially for β turns. A quite similar doublet was also observed, for instance, for the peptide L-Pro-L-Leu-Gly-NH_2,[65] which shows a β turn of type II.[66,67] Moreover, this wavenumber region has already been found in Raman spectra to be characteristic for β turns.[21]

The remaining part of the calculated spectrum does not agree well with the experimental one, which may in addition to the reasons mentioned above also be due to the fact that the α domain of the metallothionein has been omitted in our calculations. For instance, the intense positive band around 1420 cm^{-1} in the calculated spectrum is, if at all, found with a quite weak positive intensity around 1400 cm^{-1} in experiment. The subsequent negative band has its minimum at around 1460 cm^{-1}

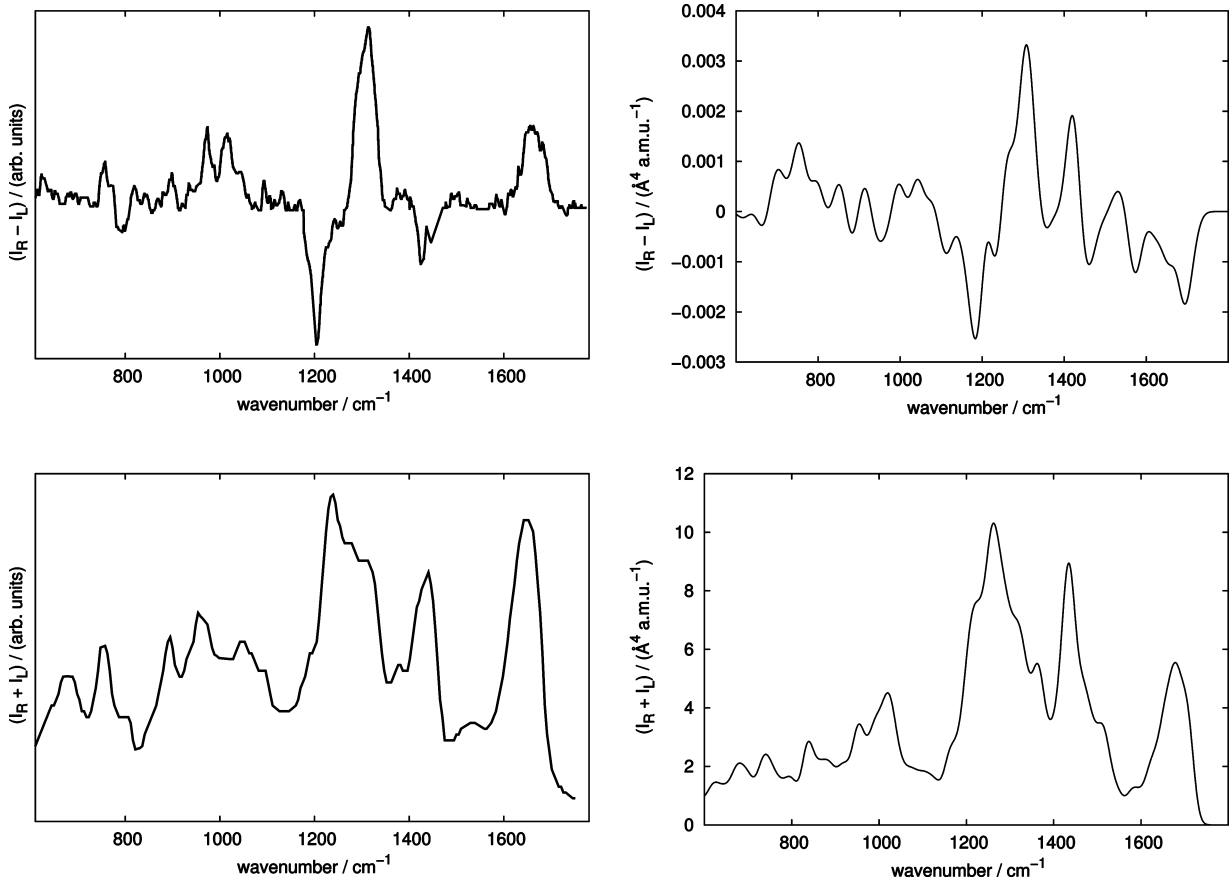

Figure 7. Experimental backscattering ROA (top, left-hand side) and Raman (bottom, left-hand side) spectra of rabbit metallothionein reproduced from ref 22; the calculated ROA (top) and Raman (bottom) spectra (BP86/RI/TZVP) of the β domain of rat metallothionein are given on the right-hand side.

in the calculated spectrum. In the experimental one, two negative bands around 1435 cm^{-1} are obtained. These may originate from methyl out-of-plane deformational vibrations, for which negative intensity values are evaluated in our calculation in this wavenumber range. The negative band at about 1575 cm^{-1} in the calculated spectrum is not observed in the experimental one. As described in the previous section, this band is due to the combination of Lys20 C−N and C═O stretching vibrations and hydrogen deformational vibrations of Ser18. It should be noted that the positions of these two residues in our model structure deviate remarkably from the ones in the crystal structure, where the distance between these residues is larger. Thus, this vibration may not necessarily exist in such a way in ROA measurements, possibly also due to solvent effects. The positive band at 1652 cm^{-1} in the experimental ROA spectrum is not found in our calculated spectrum. Indeed, several normal modes show positive intensities in the calculated spectrum, but they overlap with other negative bands, leading in total to a negative band, which is broadened to the lower wavenumber side. The minimum at 1708 cm^{-1} mainly stems from the amide I mode of Cys21 and Lys22, whereas especially NH_3 wagging modes from the Lys residues contribute around 1650 cm^{-1}. Since these Lys residues occur at the outer sphere of the metallothionein, their ROA intensities may significantly be changed if explicit solvation is considered (as has been found, e.g., for sugar molecules[44]).

Looking at the experimental and calculated Raman spectra at the bottom of Figure 7, a good agreement between both spectra is apparent. Although the relative intensities differ, the characteristic patterns are easily visible. The two bands in the region from 600 to 800 cm^{-1} are found in both spectra as well as the minimum around 820 cm^{-1} and the following band, at about 890 cm^{-1} in the measured and around 840 cm^{-1} in the calculated spectrum. The two bands centered around 1000 cm^{-1} are observed in the experimental measurement with a higher Raman intensity for the one at lower wavenumbers, whereas the band with higher wavenumbers gives rise to a more intense band in our calculation. The remaining part of the experimental spectrum with bands at around 1240 cm^{-1} (which is broadened to the higher wavenumber range), 1440 cm^{-1}, and 1650 cm^{-1} is also obtained in our calculation, although the relative intensity of the band at 1650 cm^{-1} is smaller than in the measured spectrum.

6. Conclusion

We have presented the ROA spectrum calculation of the β domain of rat metallothionein, which is by far the largest molecule for which a full ab initio calculation has been performed. The calculation has been possible due to the employment of density-fitting techniques for the ROA property tensor calculation in combination with a massive parallelization of the calculations.[41] Some characteristic ROA bands have been found in the lower wavenumber region, for instance, a positive doublet centered around 1000 cm^{-1}. The ROA spectrum is dominated by a negative band around 1200 cm^{-1}, which originates from cysteine residues ligating the metal atoms, and a positive band around 1310 cm^{-1} corresponding to amide I and C^{α}−H bending vibrations. The following bands are mainly dominated by contributions from the lysine residues, except for the amide I modes from around 1670 to 1710 cm^{-1}.

We have compared our ROA spectrum with the one obtained experimentally in solution from the rabbit metallothionein, which differs from the rat metallothionein by inclusion of seven cadmium instead of five cadmium and two zinc metal atoms. The agreement is partly quite good, especially for the characteristic negative and positive bands around 1250 cm^{-1}. Differences occur for the bands at higher wavenumbers, which may be due to the neglect of solvent effects in addition to the structural differences of the metallothioneins. In contrast to that, large similarities between the calculated and experimental Raman spectra have been detected showing clearly that the Raman spectrum is not that sensitive to possible solvent and structural effects as the corresponding ROA spectrum.

Our calculations suggest that the intense negative and positive bands at around 1200 and 1300 cm^{-1}, respectively, may serve as a signature for β turns, since our model structure contains five β turns (in addition to one γ turn) as the only secondary structure elements. A similar pattern was also observed in the measured ROA spectrum of a model β turn peptide.[65] However, in order to investigate if ROA spectroscopy is able to distinguish the different types of β turns, a more detailed study is necessary which studies the dependence of the ROA intensity on the different turns and the corresponding ψ and ϕ angles of the amino acids. Such work as well as work on the effect of water solvation on ROA signatures of protein structure is currently in progress in our laboratory.

Acknowledgment. This work was supported by the Swiss National Science Foundation (project 200020-121870).

References and Notes

(1) Bell, S. G.; Vallee, B. L. *ChemBioChem* **2009**, *10*, 55–62.
(2) Duncan, K. E.; Ngu, T. T.; Chan, J.; Salgado, M. T.; Merrifield, M. E.; Stillman, M. J. *Exp. Biol. Med.* **2006**, *231*, 1488–1499.
(3) Vallee, B. L. *Neurochem. Int.* **1995**, *27*, 23–33.
(4) Coyle, P.; Philcox, J. C.; Carey, L. C.; Rofe, A. M. *Cell. Mol. Life Sci.* **2002**, *59*, 627–647.
(5) Maret, W. *Neurochem. Int.* **1995**, *27*, 111–117.
(6) Maret, W. *J. Nutr.* **2000**, *130*, 1455S–8S.
(7) Maret, W. *Exp. Gerontol.* **2008**, *43*, 363–369.
(8) Ebadi, M.; Iversen, P.; Hao, R.; Cerutis, D. R.; Rojas, P.; Happe, H. K.; Murrin, L. C.; Pfeiffer, R. F. *Neurochem. Int.* **1995**, *27*, 1–22.
(9) Aschner, M. *Neurotoxicology* **1998**, *19*, 653–660.
(10) Li, X.; Cai, L.; Feng, W. *Mini-Rev. Med. Chem.* **2007**, *7*, 761–768.
(11) Melis, K. A.; Carter, D. C.; Stout, C. D.; Winge, D. R. *J. Biol. Chem.* **1983**, *258*, 6255–6257.
(12) Furey, W. F.; Robbins, A. H.; Clancy, L. L.; Winge, D. R.; Wang, B. C.; Stout, C. D. *Science* **1986**, *231*, 704–710.
(13) Schultze, P.; Wörgötter, E.; Braun, W.; Wagner, G.; Vašák, M.; Kägi, J. H. R.; Wüthrich, K. *J. Mol. Biol.* **1988**, *203*, 251–268.
(14) Robbins, A. H.; McRee, D. E.; Williamson, M.; Collett, S. A.; Xuong, N. H.; Furey, W. F.; Wang, B. C.; Stout, C. D. *J. Mol. Biol.* **1991**, *221*, 1269–1293.
(15) Braun, W.; Vašák, M.; Robbins, A. H.; Stout, C. D.; Wagner, G.; Kägi, J. H.; Wüthrich, K. *Proc. Natl. Acad. Sci. U.S.A.* **1992**, *89*, 10124–10128.
(16) Vašák, M. *Biodegradation* **1998**, *9*, 501–512.
(17) Keiderling, T. A. Peptide and Protein Conformational Studies with Vibrational Circular Dichroism and Related Spectroscopies. In *Circular Dichroism: Principles and Applications*; Berova, N., Nakanishi, K., Woody, R. W., Eds.; Wiley-VCH: New York, 2000.
(18) Barron, L. D.; Boogard, M. P.; Buckingham, A. D. *J. Am. Chem. Soc.* **1973**, *95*, 603–605.
(19) Hug, W.; Kint, S.; Bailey, G.; Scherer, J. R. *J. Am. Chem. Soc.* **1975**, *97*, 5589–5590.
(20) Barron, L. D. *Molecular Light Scattering and Optical Activity*, 2nd ed.; Cambridge University Press: Cambridge, 2004.
(21) Pande, J.; Pande, C.; Gilg, D.; Vašák, M.; Callender, R.; Kägi, J. H. R. *J. Biol. Chem.* **1983**, *258*, 6255–6257.
(22) Smyth, E.; Syme, C. D.; Blanch, E. W.; Hecht, L.; Vašák, M.; Barron, L. D. *Biopolymers* **2001**, *58*, 138–151.
(23) Lamparska, E.; Liégeois, V.; Quinet, O.; Champagne, B. *ChemPhysChem* **2006**, *7*, 2366–2376.
(24) Liégeois, V.; Quinet, O.; Champagne, B. *Int. J. Quantum Chem.* **2006**, *106*, 3097–3107.
(25) Pecul, M. *Chem. Phys. Lett.* **2006**, *427*, 166–176.
(26) Zuber, G.; Hug, W. *Helv. Chim. Acta* **2004**, *87*, 2208–2234.
(27) Zuber, G.; Goldsmith, M.-R.; Beratan, D. N.; Wipf, P. *ChemPhysChem* **2005**, *6*, 595–597.
(28) Ruud, K.; Helgaker, T.; Bouř, P. *J. Phys. Chem. A* **2002**, *106*, 7448–7455.
(29) Pecul, M.; Rizzo, A.; Leszczynski, J. *J. Phys. Chem. A* **2002**, *106*, 11008–11016.
(30) Herrmann, C.; Ruud, K.; Reiher, M. *ChemPhysChem* **2006**, *7*, 2189–2196.
(31) Reiher, M.; Liégeois, V.; Ruud, K. *J. Phys. Chem. A* **2005**, *109*, 7567–7574.
(32) Liégeois, V.; Quinet, O.; Champagne, B. *J. Chem. Phys.* **2005**, *122*, 214304.
(33) Liégeois, V.; Quinet, O.; Champagne, B.; Haesler, J.; Zuber, G.; Hug, W. *Vib. Spectrosc.* **2006**, *42*, 309–316.
(34) Liégeois, V.; Champagne, B. *J. Comput. Chem.* **2009**, *30*, 1261–1278.
(35) Herrmann, C.; Ruud, K.; Reiher, M. *Chem. Phys.* **2008**, *343*, 200–209.
(36) Luber, S.; Herrmann, C.; Reiher, M. *J. Phys. Chem. B* **2008**, *112*, 2218–2232.
(37) Pecul, M.; Ruud, K. *Int. J. Quantum Chem.* **2005**, *104*, 816–829.
(38) Bauernschmitt, R.; Häser, M.; Treutler, O.; Ahlrichs, R. *Chem. Phys. Lett.* **1997**, *264*, 573–578.
(39) Grimme, S. *Chem. Phys. Lett.* **2001**, *339*, 380–388.
(40) Grimme, S.; Furche, F.; Ahlrichs, R. *Chem. Phys. Lett.* **2002**, *361*, 321–328.
(41) Luber, S.; Reiher, M. *Chem. Phys.* **2008**, *346*, 212–223.
(42) Jacob, C. R.; Luber, S.; Reiher, M. *ChemPhysChem* **2008**, *9*, 2177–2180.
(43) Jacob, C. R.; Luber, S.; Reiher, M. *J. Phys. Chem. B* **2009**, *113*, 6558–6573.
(44) Luber, S.; Reiher, M. *J. Phys. Chem. A* **2009**, *113*, 8268–8277.
(45) Luber, S.; Reiher, M. *ChemPhysChem* **2009**, *10*, 2049–2057.
(46) Luber, S.; Neugebauer, J.; Reiher, M. 2009, submitted.
(47) Jacob, C. R.; Luber, S.; Reiher, M. *Chem. Eur. J.* **2009**, DOI: 10.1002/chem.200901840.
(48) Berweger, C. D.; Thiel, W.; van Gunsteren, W. F. *Proteins: Struct., Funct., Genet.* **2000**, *41*, 299–315.
(49) Bouř, P.; Baumruk, V.; Hanzlikovà, J. *Collect. Czech. Chem. Commun.* **1997**, *62*, 1384–1395.
(50) Ahlrichs, R.; Bär, M.; Häser, M.; Horn, H.; Kölmel, C. *Chem. Phys. Lett.* **1989**, *162*, 165–169.
(51) Becke, A. D. *Phys. Rev. A* **1988**, *38*, 3098–3100.
(52) Perdew, J. P. *Phys. Rev. B* **1986**, *33*, 8822–8824.
(53) Schäfer, A.; Huber, C.; Ahlrichs, R. *J. Chem. Phys.* **1994**, *100*, 5829–5835.
(54) Neugebauer, J.; Reiher, M.; Kind, C.; Hess, B. A. *J. Comput. Chem.* **2002**, *23*, 895–910.
(55) The Pymol Molecular Graphics System; http://www.pymol.org.
(56) Protein Structure Validation Suite; http://psvs-1_3.nesg.org.
(57) Davis, I. W.; Leaver-Fay, A.; Chen, V. B.; Block, J. N.; Kapral, G. J.; Wang, X.; Murray, L. W.; Bryan Arendall III, W.; Snoeyink, J.; Richardson, J. S.; Richardson, D. C. *Nucleic Acids Res.* **2007**, *35*, W375–W383.
(58) Venkatachalam, C. M. *Biopolymers* **1968**, *6*, 1425–1436.
(59) Lewis, P. N.; Momany, F. A.; Scheraga, H. A. *Biochem. Biophys. Acta* **1973**, *303*, 211–229.
(60) Richardson, J. S. *Adv. Protein Chem.* **1981**, *34*, 167–339.
(61) Hutchinson, E. G.; Thornton, J. M. *Protein Sci.* **1994**, *3*, 2207–2216.
(62) Ramachandran, G. N.; Ramakrishnan, C.; Sasisekharan, V. *J. Mol. Biol.* **1963**, *7*, 95–99.
(63) Hug, W. *Chem. Phys.* **2001**, *264*, 53–69.
(64) Jacob, C. R.; Reiher, M. *J. Chem. Phys.* **2009**, *130*, 084106.
(65) Wen, Z. Q.; Hecht, L.; Barron, L. D. *Protein Sci.* **1994**, *3*, 435–439.
(66) Reed, L. L.; Johnson, P. L. *J. Am. Chem. Soc.* **1973**, *95*, 7523–7524.
(67) Higashijima, T.; Tasumi, M.; Miyazawa, T.; Miyoshi, M. *Eur. J. Biochem.* **1978**, *89*, 543–556.
(68) Lovell, S. C.; Davis, I. W.; Arendall, W. B., III; de Bakker, P. I. W.; Word, J. M.; Prisant, M. G.; Richardson, J. S.; Richardson, D. C. *Proteins: Struct., Funct., Genet.* **2003**, *50*, 437–450.

JP909483Q